Available online at www.sciencedirect.com

SciVerse ScienceDirect

Ceramics International 39 (2013) 3921–3929

CERAMICS INTERNATIONAL

www.elsevier.com/locate/ceramint

Synthesis of hybrid compounds apatite–alendronate by reactive milling and effects on the structure and morphology of the apatite phase

Nancy Vargas-Becerril[a,*], Cristobal Patiño-Carachure[b], Luis M. Rodriguez-Lorenzo[c,d], Lucía Téllez-Jurado[a]

[a]National Politecnic Institute, E.S.I.Q.I.E. Zacatenco, 07738 México City, Mexico
[b]UNACAR Campus III 24115 Ciudad del Carmen, Campeche, México
[c]Biomaterials Group, ICTP-CSIC, Juan de la Cierva, Madrid 3 (28006), Spain
[d]Networking Biomedical Research Centre in Bioengineering, Biomaterials and Nanomedicine, CIBER-BBN, Spain

Received 14 May 2012; received in revised form 8 October 2012; accepted 22 October 2012
Available online 5 November 2012

Abstract

The preparation of apatite–alendronate hybrid materials by reactive milling is proposed in this work. Calcium phosphate compounds of various compositions have been associated to bisphosphonates and found suitable for local application with release kinetics of the drug compatible with the inhibition of bone resorption. Hybrid compounds have been obtained by reactive milling. The compositions used were: AP(X-100), Alendronate(X) where $X=7$ and $X=15$. An interaction between the hydroxyl group of the apatite and the amine group of alendronate can be identified with FTIR and enables to confirm the formation of the hybrids. The incorporation of the alendronate hinders the growing of the apatite crystals resulting in smaller coherent domains of diffraction for the apatite phase.

Keywords: D. Apatite; Alendronate; Hybrids; Reactive milling

1. Introduction

Hydroxyapatite (HAp) functions as a bioactive material that directly regulates the behavior of both normal and transformed cells [1]. For example, HAp has been shown to enhance normal bone formation and to alter growth and expression profiles of bone metastatic tumors [2]. Also, HAp can bypass a host foreign body response system and integrate with the surrounding tissues, unlike other artificial materials. The versatile apatite structure accept numerous substitutions such as K^+, Na^+, Mg^{2+}, OH^- or CO_3^{2+} (replacing to the Ca^{2+}, PO_4^{3-} and/or OH^- ions). These ions and groups may play a role on the reactivity, stability and properties of the apatite [3]. Also, hydroxyapatite has the ability to form strong chemical bonds with natural bone and a variety of molecules [4,5]. Bisphosphonates (Bps), which possess a strong affinity to hydroxyapatite under physiological conditions [6] are between those molecules with a great medical potential.

Bisphosphonates are synthetic pyrophosphate analogs, which have a P–C–P bridge and two phosphonic acid groups bonded to the same central carbon [7–9]. There are also two sides chains in the structure normally referred as $R1$ and $R2$. The biological activity and affinity to bone are defined by this structure. It is generally accepted than the $R1$ side chain determines the binding to bone mineral and the cellular effects depend on the $R2$ side chain [10–12]. The bisphosphonates are widely used drugs for the treatments in bone disorders, such as osteoporosis, Paget's desease or hypercalcemia [10].

The Bps are currently administered orally, but their absorption is very poor (about 1% of administered dose) and only the 20% of the absorbed compound is incorporated into bone. Consequently, other administration routes such as nasal delivery, subcutaneous or intramuscular injection have been developed [13,14]. The main goal for these drugs is their in situ administration, avoiding in this way the side effects associated with conventional systemic

*Corresponding author. Tel.: +52 55 538 200 09.
E-mail addresses: lennon_nancy@hotmail.com, nanxyvb@gmail.com (N. Vargas-Becerril).

0272-8842/$ - see front matter © 2012 Elsevier Ltd and Techna Group S.r.l. All rights reserved.
http://dx.doi.org/10.1016/j.ceramint.2012.10.239

therapy. Calcium phosphate compounds of various compositions have been associated to Bps and found suitable for local application with release kinetics of the drug compatible with the inhibition of bone resorption [15].

In this paper, we proposed the preparation of HAp–Bp hybrid materials by reactive milling and to study the effects of the incorporation of alendronate on the structure of different apatites. Apatites with different features have been prepared by a co-precipitation route with both mechanical and ultrasonic stirring. Then hybrids compounds were obtained by reactive milling.

2. Materials and methods

Apatites were synthesized by a coprecipitation method assisted either by mechanical stirring or ultrasound stirring. The hydroxyapatite was prepared from two aqueous solutions; The first solution was prepared with 8 mL of H_3PO_4 (85% J.T.-Baker)+235 mL deionized water, which it was added dropwise to a second aqueous solution, prepared with 14.75 g $Ca(OH)_2$ (Sigma-Aldrich)+200 mL deionized water. Powders were washed with distiller water and dried at 100 °C during 24 h. While the synthesis assisted by mechanical stirring was maintained for 20 h (sample identified as Ap1), the synthesis assisted by ultrasound stirring was maintained for 0.5 h at ~35 °C (sample Ap2). Hybrid compounds were obtained by reactive milling in a RETCH MM400 mill with a setting of vibrational frequency of 30 Hz. Powders of apatite and alendronate (Sigma-Aldrich) were mixed for 45 min. The compositions used were: $AP_{(X-100)}$, $Alendronate_{(X)}$ where $X=7$ and $X=15$ and it refers to the percentage of alendronate. The names for the hybrid compounds are Ap1–A7 Ap2–A7 for the hybrids with 7% of alendronate, and Ap1–A15 Ap2–A15 with a 15% of alendronate. The apatites were also subjected to the same process free of bisphosphonate and were identified as Ap1-0 and Ap2-0.

The apatites and hybrid compounds were analysed in a Bruker D8 Advance with CuK_α ($\lambda=1.54$ Å) radiation, and with a diffraction angle (2θ) range between 5° to 60°, and the structural analysis was performed by FullPROF suite. A Perkin–Elmer Spectrum One apparatus was utilized for registering the ATR–IR spectra, in order to know the absorption bands that correspond to the apatite and alendronate, as well as to prove the interaction between both. The specific surface area of the apatites Ap powders was evaluated by the Brunaer–Emmett–Teller method in a Bell Prep II-Belsorp II, Bell Japan Inc. Thermal properties were studied in a TGA instrument Q500 with a heating rate to 10 °C min^{-1} and a maximum temperature of 800 °C. The morphology and microstructure was analized by a Field Emission Scanning Electron Microscopy SEM model JEOL JSM-670IF.

3. Results and discussion

The X-ray diffractions patterns obtained from Ap1 (Fig. 1(a)) and Ap2 (Fig. 1(b)) show the characteristic peaks

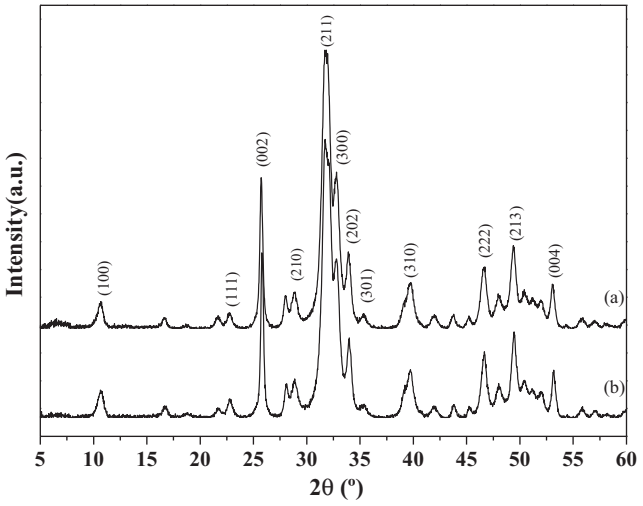

Fig. 1. X-ray diffractograms of apatite obtained by co-precipitation rute: (a) Ap1 and (b) Ap2.

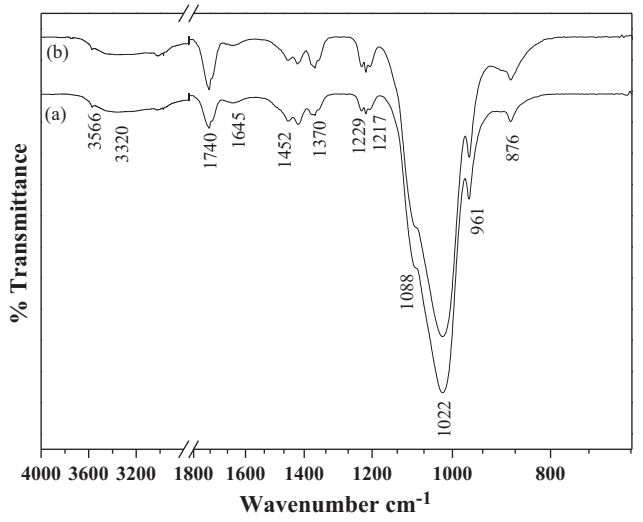

Fig. 2. ATR–IR spectra from apatites obtained by co-precipitation route: (a) Ap1 and (b) Ap2.

of a hydroxyapatite phase according to the crystallographic letter JCDS-9-0432, no secondary phases could be detected. ATR–IR spectra obtained (Fig. 2(a) and (b)), are similar and they show the characteristic absorption bands of hydroxyapatite; the bands of the PO_4^{3-} group are observed about at 1088 cm^{-1} and 1022 cm^{-} in both spectra Ap1 and Ap2. They arise from a triply degenerate stretching vibration mode v_3 [16–19]. The bands about at 961 cm^{-1} for both, Ap1 and Ap2 spectra, belong to the vibration mode v_1 [16–19]. The broad bands about at 3566, 3320 and 1645 cm^{-1} for Ap1 and Ap2 spectra is due to adsorbed water [16,18,19]. The bands about at 1452, 1422 and 876 cm^{-1} for Ap1 and Ap2, which indicate the presence of CO_3^{-2}, substituting to PO_4^{3-} in the apatite lattice [16,19,20], indicating that both synthetized apatites are carbonated apatites of the β-type [21]. The bands located between 1229–1217 cm^{-1} that correspond to HPO_4^{2+}, these

bands are characteristic of the apatites obtained at low temperatures [22,23]. The band at $\sim 1740\ cm^{-1}$ for Ap1 and Ap2 correspond to the C–O bond of CO_2 [24] as result of the ATR–IR technique.

The parameters for Ap1 are $a=9.40478$ and $c=6.87533$, which are greater than carbonate free hydroxyapatite, whereas for Ap2 are $a=9.44456$ and $c=6.88634$. It is well known that preparation conditions have a marked influence on the c and particularly a-axis on apatites with carbonate content [25] and the ultrasonic stirring should be made responsible for the change in the cell parameter rather than the carbonate content itself.

Crystal sizes are 12.339110 nm for a-axis and 18.652337 nm for c-axis on Ap1 and 11.257452 and 16.862285 nm for Ap2. The micrograph obtained from Ap1 (Fig. 3(a)) shows spherical particles with a size between 20 nm and 50 nm, whereas in the micrograph from Ap2 (Fig. 3(b)) shows elongated particles with a particle size between 10 and 50 nm. SSA for Ap1 and Ap2 are 72 and 60 cm^2/g, respectively. The particle size observed in the SEM for Ap2 is smaller than the observed for Ap1. This fact can be due to an acoustic cavitation effect [26,27]. Apatite ceramics prepared by the conventional sintering furnace are made through a slow heating rate that leads to the growth and enlargement of crystal grains. On the contrary, microwave sintering has a fast heating rate and can be used for the fabrication of nanosized or submicrosized ceramics [28]. Fig. 4 shows the thermogravimetric analysis curves from Ap1 and Ap2. The curve from Ap1 has a continuous weight loss and the total weight loss is at 6.7% at 800 °C. The event before 570 °C could be due to the removal of adsorbed and structural water, and at 630 °C can be attributed to the elimination of carbonate in CO_2 form. No other significant events are observed up to 800 °C for Ap1 and Ap2.

The biological performance of a biomaterial is related tightly with its structure and property. A large number of studies have shown that the microstructure of calcium phosphate ceramics played a key role in their bioactivity and osteoinduction [29,30]. On the other hand, the bisphosphonates have the ability to bind to the bone mineral, acting mainly on remodeling zones, then are absorbed by osteoclasts inhibiting the bone resorption [31,32]. New evidences suggest that the Ap–Bps interaction is more complex that though previously, including the

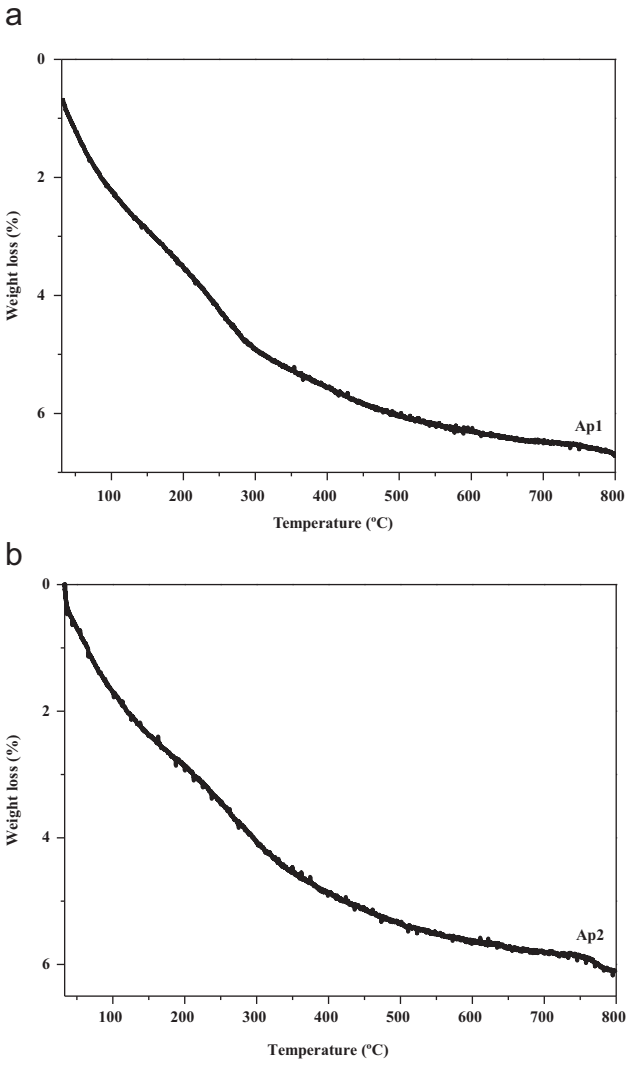

Fig. 4. (a) Thermogravimetric analysis of Ap1. (b) Thermogravimetric analysis of Ap2.

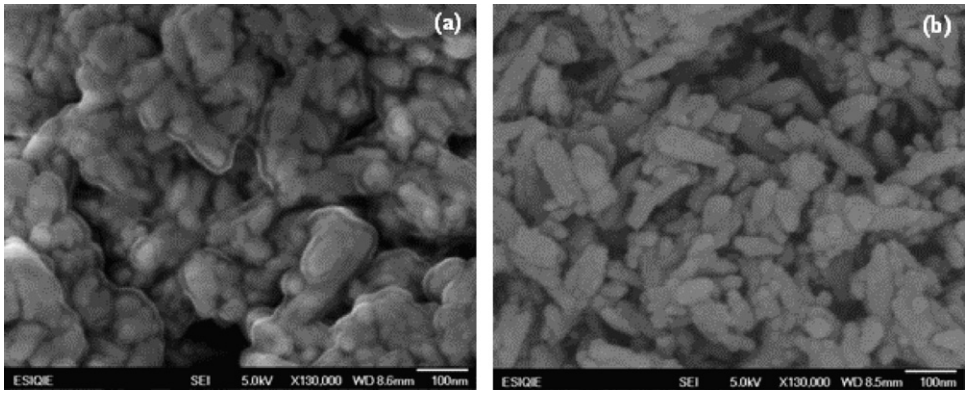

Fig. 3. SEM micrographs of apatites (a) Ap1 and (b) Ap2.

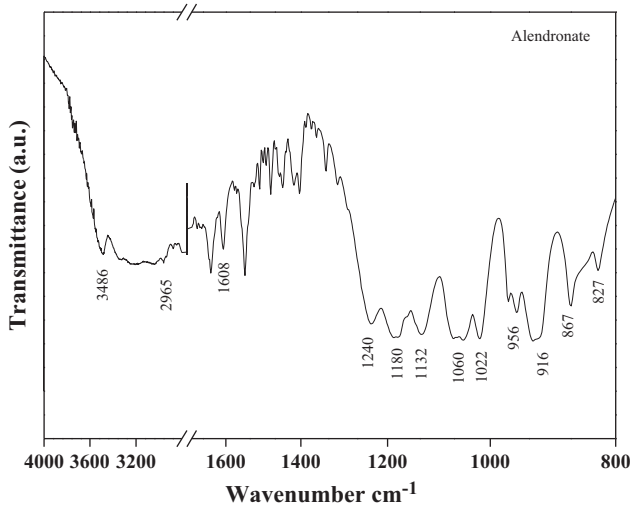

Fig. 5. ATR–IR spectrum from alendronate™.

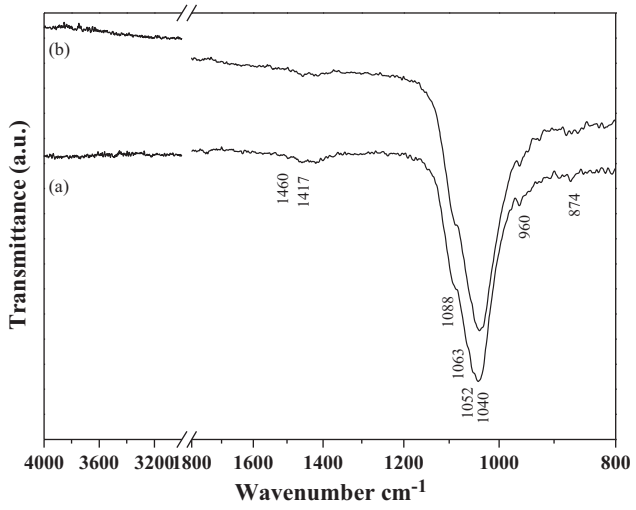

Fig. 6. ATR–IR spectra from (a) Ap1-0 and (b) Ap2-0.

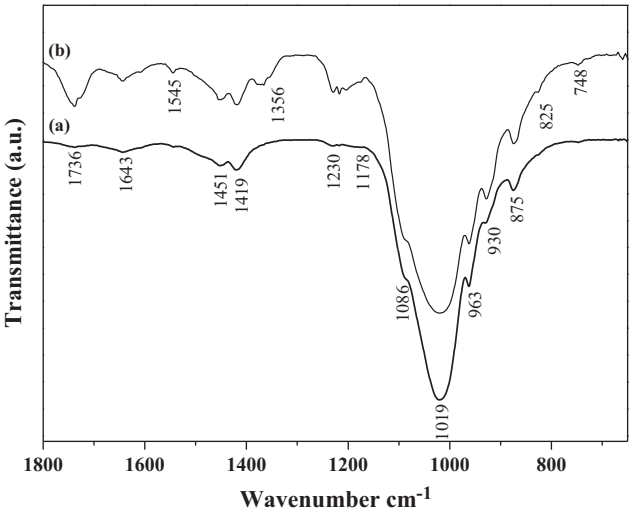

Fig. 7. ATR–IR spectra of hybrid compounds (a) Ap1–A7 and (b) Ap1–A15.

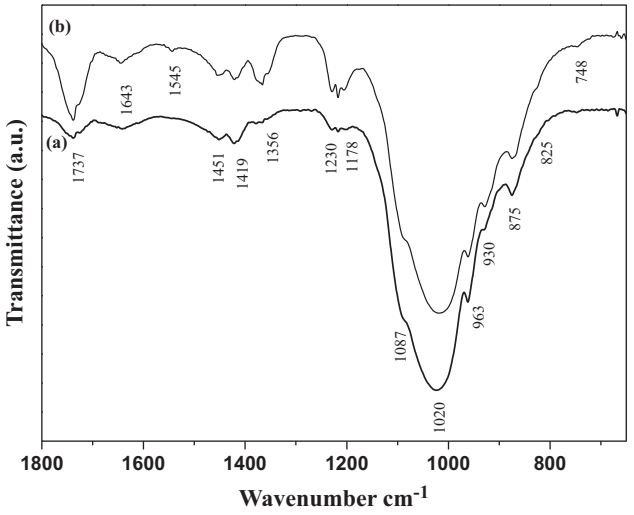

Fig. 8. ATR–IR spectra of hybrid compounds of (a) Ap2–A7 and (b) Ap2–A15.

displacement of inorganic phosphate groups by PO_3 groups from the Bp. Thus composition and textural parameters of the apatite should play a role in this interaction [33]. In this paper, a study of the interaction of alendronate with carbonated apatite with different features follows.

The IR spectrum obtained from the alendronate™ is shown in Fig. 5. The spectrum shows a band at 3486 cm^{-1} that can be assigned to the N–H group [9]. A C–H vibration mode can be assigned at 2965 cm^{-1} [34]. The band at 1608 cm^{-1} should correspond to the C=C double bond [34]. The bands at 1240, 1180 and 1132 cm^{-1} are attributed to the P=O and P–O modes [9,34,35]. A symmetric P–OH vibration mode is located at 1060 cm^{-1} and the bands at 1022, 956 and 916 cm^{-1} belong to the asimmetric vibration of P–OH [35,36]. Also, the asimmetric vibration of the POP group is located at 867 cm^{-1} and the P–OH vibration mode is located at 827 cm^{-1} [36].

The ATR–IR spectra from the apatites with/without alendronate™ are shown in the next figures. ATR–IR spectra from Ap1-0 and Ap2-0 (Fig. 6), show the characteristics bands of the hydroxyapatite; the bands in the region of 1088 to 1040 cm^{-1} are due to v_3 vibrational mode of PO_4^{3-} group and the band located about 960 cm^{-1} correspond to the v_1 vibrational mode of PO_4^{3-} group [37,38]. The bands between 1460 to 1417 are due to the v_3 vibrational mode of CO_3^{2-} ion and ~874 cm^{-1} are attributed to the v_2 vibrational mode of CO_3^{2-} ion [37,39]. Hybrid compounds spectra (Figs. 7 and 8) indicate the presence of bands that identify the interaction between the apatite and the alendronate. The bands located at 1545 and 1356 cm^{-1} could be assigned to the N=O bond in both spectra, this bond is between the hydroxyl group of apatite and the amine group of alendronate.

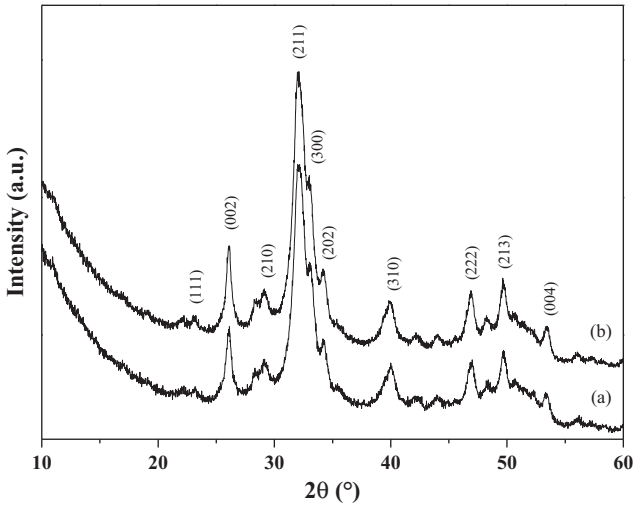

Fig. 9. X-ray difractograms from (a) Ap1-0 and (b) Ap2-0.

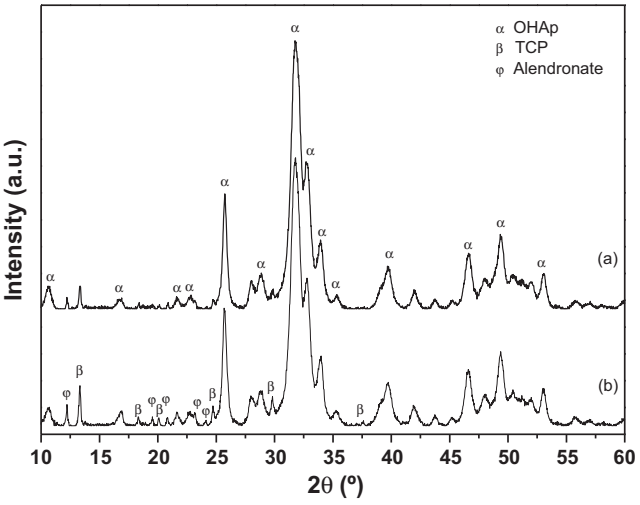

Fig. 10. X-ray diffractograms from (a) Ap1–7 and (b) Ap1–A15.

This interaction has been described thought 3-D computational modeling; the interaction between an bisphosphonate at the calcium Ca(1) site where the bidentate and tridentate coordination of the P–C–P and *R*1–OH domains of the bisphosphonate interact [40]. This explains how the *N*-bisphosphonate interacts on the hydroxyapatite surface to form N–H–O bonds. Other band located at 930 cm^{-1} that is assigned to the P–O bond and could be related to the deprotonation of the phosphonate group can be identified as well [34]. Also, another band located at 748 cm^{-1} is assigned to the $–CH_2$ modes of the absorbed alendronate [41].

The X-ray diffractograms corresponding to Ap1-0 and Ap2-0 (Fig. 9) show the stability of hydroxyapatite after being subjected to 45 min of grinding. No secondary phases can be identified whereas the X-ray diffractograms of the hybrids compounds Ap1–A7, Ap1–A15 (Fig. 10), and Ap2–A7–A15 (Fig. 11), show two extra phases. They correspond to a *β*–TCP phase (β–$Ca_3(PO_4)_2$) according to

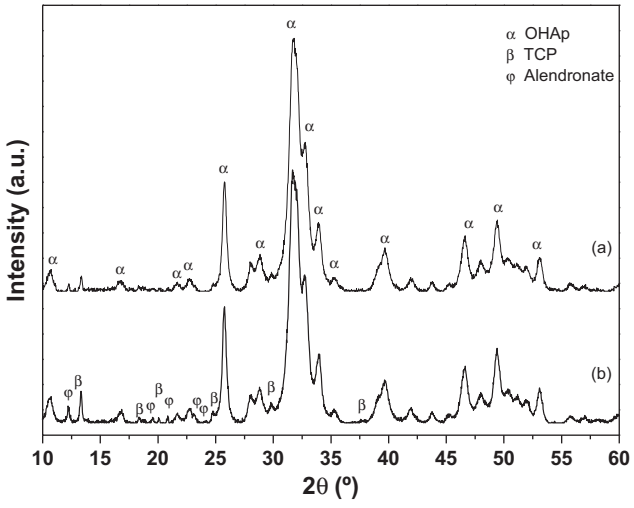

Fig. 11. X-ray diffractograms of the hybrids compounds (a) Ap2–A7 and (b) Ap2–A15.

Table 1
Cell parameters from the apatites and hybrid compounds.

Sample	Parameter *a* (Å)	Parameter *c* (Å)
Ap1	9.40478 ± 0.00078	6.87533 ± 0.00060
Ap1-0	9.55110 ± 0.00385	6.98315 ± 0.00282
Ap1–A7	9.33183 ± 0.00558	6.82571 ± 0.00395
Ap1–A15	9.38992 ± 0.00100	6.86565 ± 0.00080
Ap2	9.44456 ± 0.00101	6.88634 ± 0.00077
Ap2-0	9.67286 ± 0.00381	7.05729 ± 0.00279
Ap2–A7	9.38851 ± 0.00618	6.85265 ± 0.00436
Ap2–A15	9.41478 ± 0.00599	6.86851 ± 0.00423

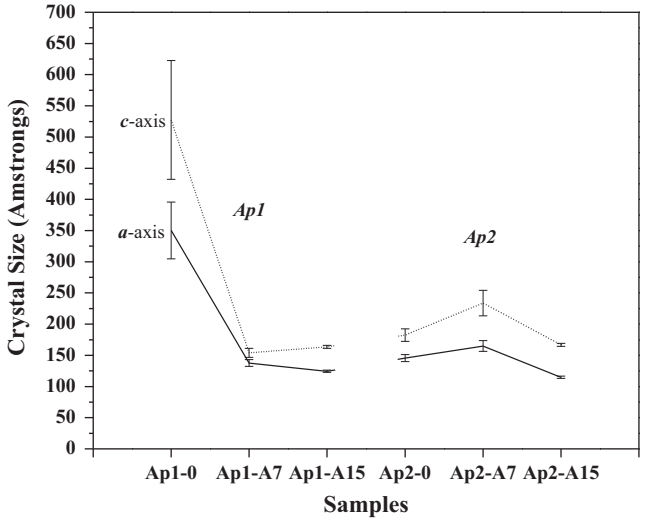

Fig. 12. Crystal size of apatite and hybrid compounds.

JCPDS 70-2065, peaks at 2*θ* 13.34, 18.4, 19.57, 20.05, 29.80 and 37.53° and to the alendronate phase at 2*θ* 9.05, 12.25, 19.57, 20.81, 23.15, 24.10 and 24.70°. Lattice parameters Ap1-0 and Ap2-0 (Table 1) show an increase in *c*-axis and *a*-axis compared to Ap1 and Ap2, even

greater apatite parameters CO_3 free. This increase in the lattice parameters is due to an increase in the degree of crystallization in both apatites. In comparison to the Ap used for the preparation of the hybrids a decrease in lattice parameters of *a*- and *c*-axis is observed for both Ap1–A7 and Ap2–A7, (Table 1). Cell parameters are also smaller for Ap1–A15 and Ap2–A15 but larger than in their corresponding A7 compounds. While in compared with Ap1-0 and Ap2-0, the cell parameters are smallest; this due to the interaction of the apatite bisphosphonate. A similar behavior can be appreciated for the coherent domain of diffraction of the apatite component (Fig. 12). It is smaller for the hybrids with a 7% of alendronate along the *c*-axis than for hybrids with a 15% of alendronate and in both cases is smaller than for Ap. The contrary can be observed for the domain along the *a*-axis. Fig. 13 shows the lattice strain variation of the apatite structure where the % strain from Ap1 increases with the decrease of domains and the % strain from Ap2 increases with the increase of domains. With these results shown in Fig. 13, it can be said that the smaller the size difference between the domains is, the lower stress in the structure is obtained.

Termogravimetric curves from Ap1–A7 and Ap1–A15 (Fig. 14(a)), have a total weight loss of 10.4 and 12.5%, respectively. Ap2–A7 and Ap2–A15 (Fig. 14(b)), show a weight loss at 800 °C of 11.2 and 12.5%, respectively. For the hybrid compounds, a loss of stability is observed at 725 °C which could be due to the removal of OH groups from apatite lattice [42]. Elisa Boanini et al. [8] refer to the effect of alendronate on the thermal stability of hybrid compound apatite-bisphosphonate which lead to a partial conversion into β-tricalcium phosphate as observed in the X-ray difraction patterns (Figs. 10 and 11). Also the amount of β–TCP can be correlated with the amount of the alendronate content.

Micrographs from apatites Ap1-0 and Ap2-0 (Fig. 15(a) and (b)) show the formation of large agglomerates of particles as a result of particle size reduction. The particle sizes, in both cases, are greater than 5 nm and less than 50 nm. The observed morphology remains Ap1-0 spherical, whereas in the case of Ap2-0 the morphology changed from elongated particle morphology to spherical particle. In the case of the micrographs (Fig. 15(c) and (d)) Ap1–A7 and Ap2–A7 respectively show agglomerated particles with an apparent order in their arrangement. In these micrographs can be seen agglomerates formed by nanosized spherical particles smaller than Ap1 and Ap2 particles, but the size is the same that can be seen in Ap1-0 and Ap2-0. The micrographs of Ap1–A15 and Ap2–A15 samples (Fig. 15(e) and (f)) show agglomerates formed without a specific order in their arrangement and they are larger than previous agglomerates. The morphology of the agglomerates is irregular and they are formed by >100 nm nanoparticles.

The agglomeration of particles seems to be favored by the morphology of the apatites. The spherical morphology of Ap1 provides a larger contact area than the morphology of elongated particles presented in Ap2.

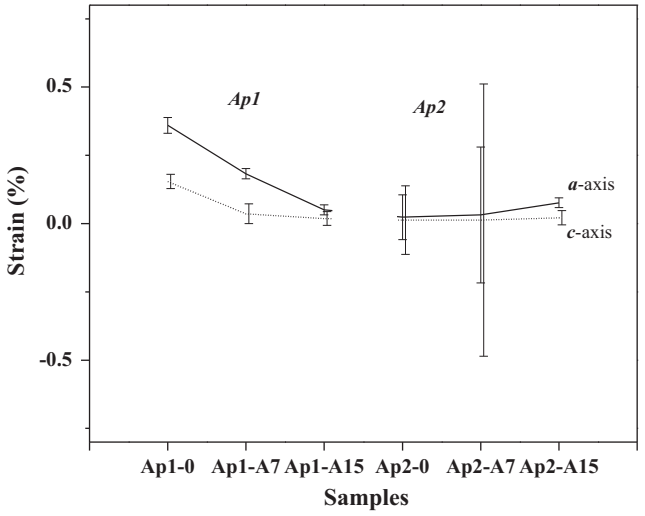

Fig. 13. % strain of apatite and hybrid compounds.

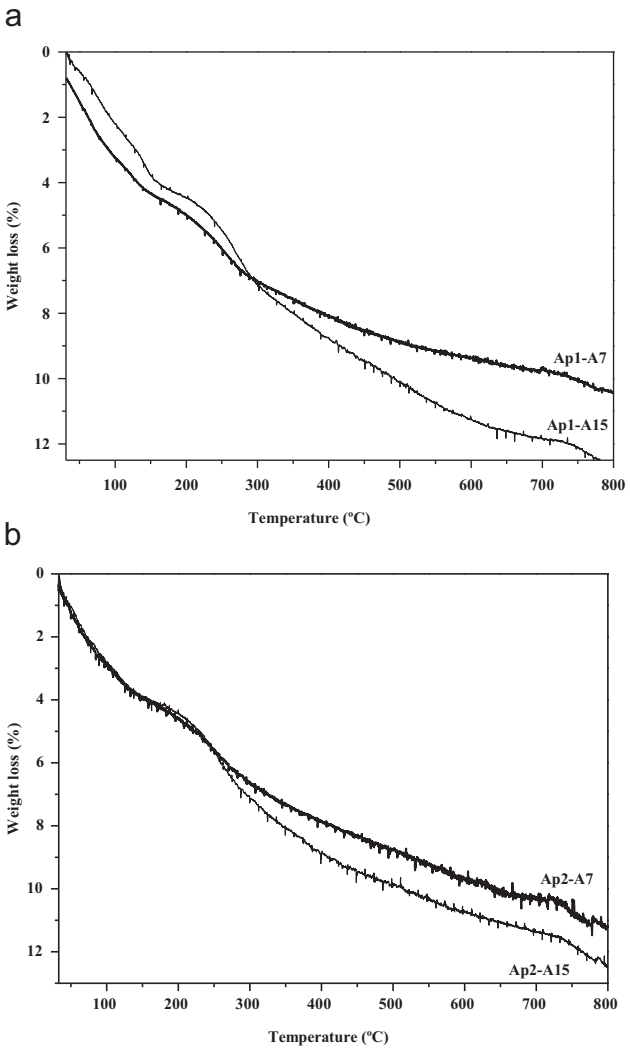

Fig. 14. (a) Thermogravimetric analysis of hybrid compounds Ap1–A7 and Ap1–A15. (b) Thermogravimetric analysis of hybrid compounds Ap2–A7 and Ap2–A15.

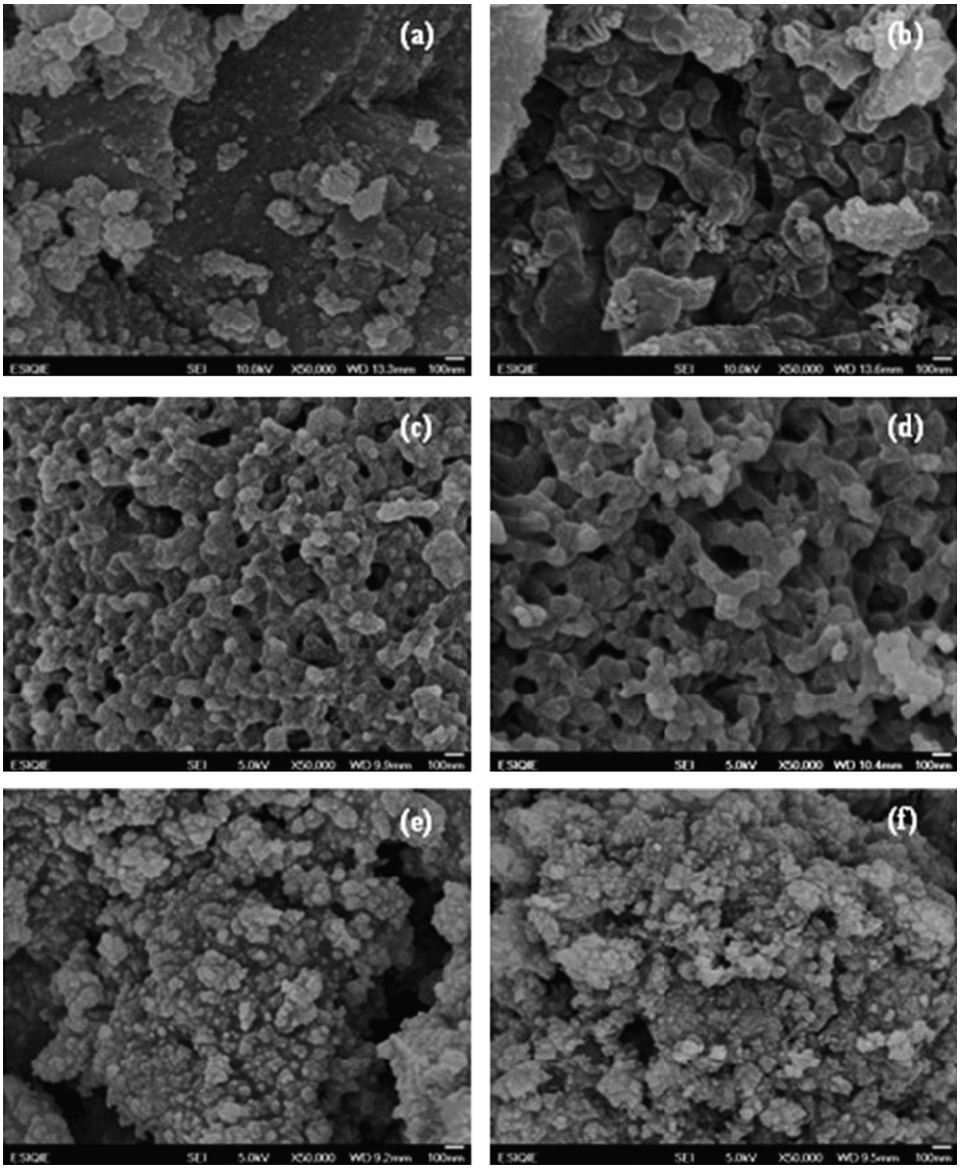

Fig. 15. SEM Micrographs from the powders: (a) Ap1-0, (b) Ap2-0, (c) Ap1–A7, (d) Ap2–A7, (e) Ap1–A15 and (f) Ap2–A15.

The apatite structure grows initially along the *c*-axis forming columns of Ca(1) surrounded by oxygen forming triangles, then these columns are linked through P–O bridges formed with oxygen from two adjacent columns. If the Bp interacts with the Ca ions, or with the OH groups of the apatite, as observed in this work, it can hinder the growing of the crystals resulting in smaller coherent domains of diffraction for the apatite phase as observed for compound with 7% alendronate content. The greater inhibition in the initial stages of the crystal growth that occur for the compounds with 15% content of alendronate may result in less crystal growth points allowing the crystals to grow a bit larger but in a less organized manner.

The hybrid Ap1–A7 shows little dispersion of agglomerates. However, for the hybrid Ap2–A7 the dispersion between the agglomerates is greater. This can be justified from the milling processes, which introduces defects and dislocations in the structure, causing a strain responsible for the decreasing of the size of the particles [43]. These defects facilitate the binding between particles due to the higher surface energy of the particles. Furthermore, the initial morphology of apatites may also play an important role in the microstructure obtained in the hybrid, since the greater contact area favors the union between them. In the case of the hybrids that contain 15% of alendronate, the formation of agglomerates is favored by the same conditions. The formation of the hybrids depends on the amount of OH^- and Ca^{2+} that are exposed on the surface of the structure of the apatite, which bind to the OH^- and N of the amine contained in the bisphosphonate. As there are a greater number of them, a greater number of bonds can be formed.

4. Conclusions

The use of ultrasonic energy in the synthesis of apatites enables to prepare hydroxyapatite in a shorter time and

produces smaller crystals than conventional stirring. The reactive milling process introduces defects and dislocations in the apatite structure and a decrease on the particle size on apatite powders favoring the formation of apatite–alendronate hybrids. The incorporation of the alendronate hinders the growing of the apatite crystals resulting in smaller coherent domains of diffraction for the apatite phase. An interaction between the apatite and alendronate can be achieved with the energy provided by the reactive milling process.

Acknowledgments

The authors thank the financial support from CONACyT, the National Politecnic Institute IPN, Mexico City, and the Science and Technology Institute of Polymers ITCP, Madrid Spain, for their support and for providing the necessary tools to do this work through CICYT project MAT2010-18155.

References

[1] G. Balasundaram, M. Sato, T.J. Webster, Using hydroxyapatite nanoparticles and decreased crystallinity to promote osteoblast adhesion similar to functionalizing with RGD, Biomaterials 27 (14) (2006) 2798–2805.

[2] S.P. Pathi, D.D.W. Lin, J.R. Dorvee, L.A. Estroff, C. Fischbach, Hydroxyapatite nanoparticle-containing scaffolds for the study of breast cancer bone metastasis, Biomaterials 32 (22) (2011) 5112–5122.

[3] S. Chakraborty, S. Bag, S. Pal, A.K. Mukherjee, Structural and microstructural Characterization of bioapatites and synthetic hydroxyapatite using X-ray powder diffraction and Fourier transform infrared techniques, Journal of Applied Crystallography 39 (2006) 385–390.

[4] S.H. Zhu, B.Y. Huang, K.C. Zhou, S.P. Huang, F. Liu, Y.M. Li, Z.G. Xue, Z.G. Long, Hydroxyapatite nanoparticles as a novel gene carrier, Journal of Nanoparticle Research 6 (2004) 307–311.

[5] T.M. Sridhar, T.K. Arumugam, S. Rajeswari, M. Subbaiyan, Electrochemical bahaviour of hydroxyapatite-coated stainless steel implants, Journal of Materials Science Lettters 16 (1997) 1964–1966.

[6] J.E.I. Wright, L. Zha, P. Choi, H. Uludag, Simulating hydroxyapatite binding of bone-seeking bisphosphonate, Biomaterials (2004) 139–148.

[7] E. Maltezou, M. Stylianou, S. Roy, C. Drouza, A.D. Keramidas, Synthesis, solutions and structural characterization of tetrahydrofuranyl-2, 2-bisphosphonic acid disodium salt, Bioinorganic Chemistry and Applications (2010) 1–7.

[8] E. Boanini, M. Gazzano, K. Rubini, A. Bigi, Composite nanocrystals provide new insight on alendronate interaction with hydroxyapatite structure, Advanced Materials 19 (2007) 2499–2502.

[9] L.M. Rodriguez-Lorenzo, B. Vazquez, J. San Roman, Surface modification of calcium hydroxyfluor carbonate apatites by bisphosphonates, Key Engineering Materials 284–286 (2005) 357–360.

[10] T.J. Martin, V. Grill, Bisphosphonates-mechanisms of action, Australian Prescriber 23 (6) (2000) 130–132.

[11] F.P. Coxon, K. Thompsom, M.J. Rogers, Recent advances in understanding the mechanism of action of bisphosphonate, Current Opinion in Pharmacology 6 (2006) 307–312.

[12] H. Fleisch, Development of bisphosphonates, Breast Cancer Research 4 (2002) 30–34.

[13] A. Ezra, G. Golomb, Administration routes and delivery systems of bisphosphonates for the treatment of bone resorption, Advanced Drug Delivery Reviews 42 (2000) 175–195.

[14] S. Patashnik, L. Rabinovich, G. Golomb, Preparation and evaluation of chitosan microspheres containing bisphosphonates, Journal of Drug Targeting 4 (1997) 371–380.

[15] S. Josse, C. Faucheux, A. Soueidan, G. Grimandi, D. Massiot, B. Alonso, P. Janvier, S. Laïb, P. Pilet, O. Gauthier, G. Daculsi, J. Guicheux, B. Bujoli, J.M. Bouler, Novel biomaterials for bisphosphonate delivery, Biomaterials 26 (2005) 2073–2080.

[16] C.C. Silva, A.G. Pinhero, M.A.R. Miranda, J.C. Góes, A.S.B. Sombra, Structural propierties of hydroxyapatite obtained by mechanosynthesis, Solid State Science 5 (2003) 553–558.

[17] M.A. Martins, C. Santos, M.M. Almeida, M.E.V. Costa, Hydroxyapatite micro- and nano-particles: nucleation and growth mechanisms in the presence of citrate species, Journal of Colloid and Interface Science 318 (2008) 210–216.

[18] M.P. Mahabole, R.C. Aiyer, C.V. Ramakrishna, B. Sreedhar, R.S. Khairnar, Synthesis, characterization and gas sensing property of hydroxyapatite ceramic, Bulletin of Material Science 28 (6) (2005) 535–545.

[19] M. Sadat-Shojai, Preparation of hydroxyapatite nanoparticles: comparison between hydrothermal and solvo-treatment processes and colloidal stability of produced nanoparticles in a dilute experimental dental adhesive, Journal of Iranian Chemical Society 6 (2) (2009) 386–392.

[20] M. Mathew, S. Takagi, Structures of biological minerals in dental research, Journal of Research of the National Institute of Standards and Technology 106 (2001) 1035–1044.

[21] A. Balamurugan, J. Michel, J. Fauré, H. Benhayoune, L. Wortham, G. Sockalingum, V. Banchet, S. Bouthors, D. Laurent-Maquin, G. Balossier, Synthesis and structural analysis of sol gel derived stoichiometric monophasic hydroxyapatite, Ceramic–Silikáty 50 (1) (2006) 27–31.

[22] S. Lazic, S. Zec, N. mIljevic, S. Milonjic, The effect of temperature on the properties of hydroxyapatite precipitated from calcium hydroxide and phosphoric acid, Thermochimic Acta 374 (2001) 13–22.

[23] G. Gafni, D. Septier, M. Goldberg, Effect of chondroitin sulfate and biglycan on the crystallization of hydroxyapatite under physiological conditions, Journal of Crystal Growth 205 (1999) 618–623.

[24] 〈www.unav.es/organica/docencia/espectroscopia_d/…/Infrarrojo.pdf〉 April 18, 2012.

[25] J.C. Elliott, Structure and Chemistry of the Apatites and Other Calcium Orthophosphates, Elsevier, Amsterdam, 1994.

[26] A.B. Martinez, G. Carbajal, R. Torres, L. Tellez, H.E. Esparza, Production of polyurethane/nano-hydroxyapatite hybrid materials and microstructural characterization, Int. J. Phys. Sci. 6 (11) (2011) 2731–2743.

[27] M. de Campos, F.A. Muller, A.H.A. Bressiani, J.C. Bressiani, P. Greil, Sonochemical synthesis of calcium phosphate powders, Journal of Materials Science: Materials in Medicine 18 (2007) 669–675.

[28] X.D. Zhu, H.J. Zhang, D.X. Li, H.S. Fan, X.D. Zhang, Study on the enhanced protein adsorption of microwave sintered hydroxyapatite nanoceramic particles: role of microstructure, Journal of Biomedical Materials Research Part B 100 (B) (2012) 516–523.

[29] M. Tamai, K. Isama, R. Nakaoka, T. Tsuchiya, Synthesis of a novel β-tricalcium phosphate/hydroxyapatite biphasic calcium phosphate containing niobium ions and evaluation of its osteogenic properties, Journal of Artificial Organs 10 (2007) 22–28.

[30] W. Paul, C.P. Sharma, Development of porous spherical hydroxyapatite granules: application towards protein delivery, Journal of Materials Science: Materials in Medicine 10 (1999) 383–388.

[31] K. Olson, C. Van Poznak, Significance and impact of bisphosphonate-induced acute phase responses, Journal of Oncology Pharmacy Practice 13 (2007) 223–229.

[32] M.A. Günther Sillero, A. de Diego, E. Silles, F. Pérez-Zuñiga, A. Sillero, Synthesis of bisphosphonate derivatives of ATP by T4 RNA ligase, FEBS Letters 580 (2006) 5723–5727.

[33] A. Juillard, G. Falgayrac, B. Cortet, M.-H. Vieillard, N. Azaroual, J.-C. Hornez, G. Penel, Molecular interactions between zoledronic

acid and bone: an in vitro Raman microspectroscopic study, Bone 47 (2010) 895–904.

[34] M.A. Bayle, K. Nasr, G. Grégoire, P. Sharrock, Acrylophosphonic acid reactivity with calcium ions and biological apatite, Dental Materials 24 (2008) 386–391.

[35] F. Al-Ali, A. Lebugle, I. Rico-Lattes, G. Etemad-Moghadam, Preparation and characterization of new hybrid organic/inorganic systems derived from calcium (α-aminoalkyl)-phosphonates and-phosphonocarboxylates, Journal of Colloid and Interface Science 289 (2005) 504–511.

[36] L.M. Rodriguez-Lorenzo, M. Fernandez, J. Parra, B. Velazquez, A. Lopéz-Bravo, J. San Romàn, Acrylic injectable and self-curing formulations for the local release of bisphosphonates in bone tissue, Journal of Biomedical Materials Research Part B: Applied Biomaterials (2007) 596–608.

[37] I. Rehman, W. Bonfield, Characterization of hydroxyapatite and carbonated apatite byn photo acoustic FTIR spectroscopy, Juornal of Material Science: Materials in Medicine 8 (1997) 1–4.

[38] Y. Han, X. Wang, S. Li, A simple route to prepare stable hydroxyapatite nanoparticles suspension, Journal of Nanoparticle Research 11 (2009) 1235–1240.

[39] M. Okada, T. Furuzono, Fabrication of high-dispersibility nanocrystals of calcined hydroxyapatite, Journal of Materials Science 41 (2006) 6134–6137.

[40] R.G.G. Russell, N.B. Watts, F.H. Ebetino, M.G. Rogers, Mechanisms of action of bisphosphonates: similarities and differences and their potential influence on clinical efficacy, Osteoporos International 19 (2008) 733–759.

[41] H. Agougui, A. Aissa, S. Maggi, M. Debbabi, Phosphonate-hydroxyapatite hybrid compounds prepared by hydrothermal method, Applied Surface Science 257 (20109) 1377–1382.

[42] X.-F. Xiao, R.-F. Liu, Y.-J. Gao, Hydrothermal preparation of nanocarboted hydroxyapatite crystallites, Material Science Technology 24 (2008) 1199–1203.

[43] C.C. Koch, Top-down synthesis of nanostructured materials: mechanical and thermal processing methods, Reviews on Advanced Materials Science 5 (2003) 91–99.